National Research Council Canada
Conseil national de recherches Canada

EVALUATION OF SOIL STRENGTH MEASUREMENTS

BY
J. Y. WONG

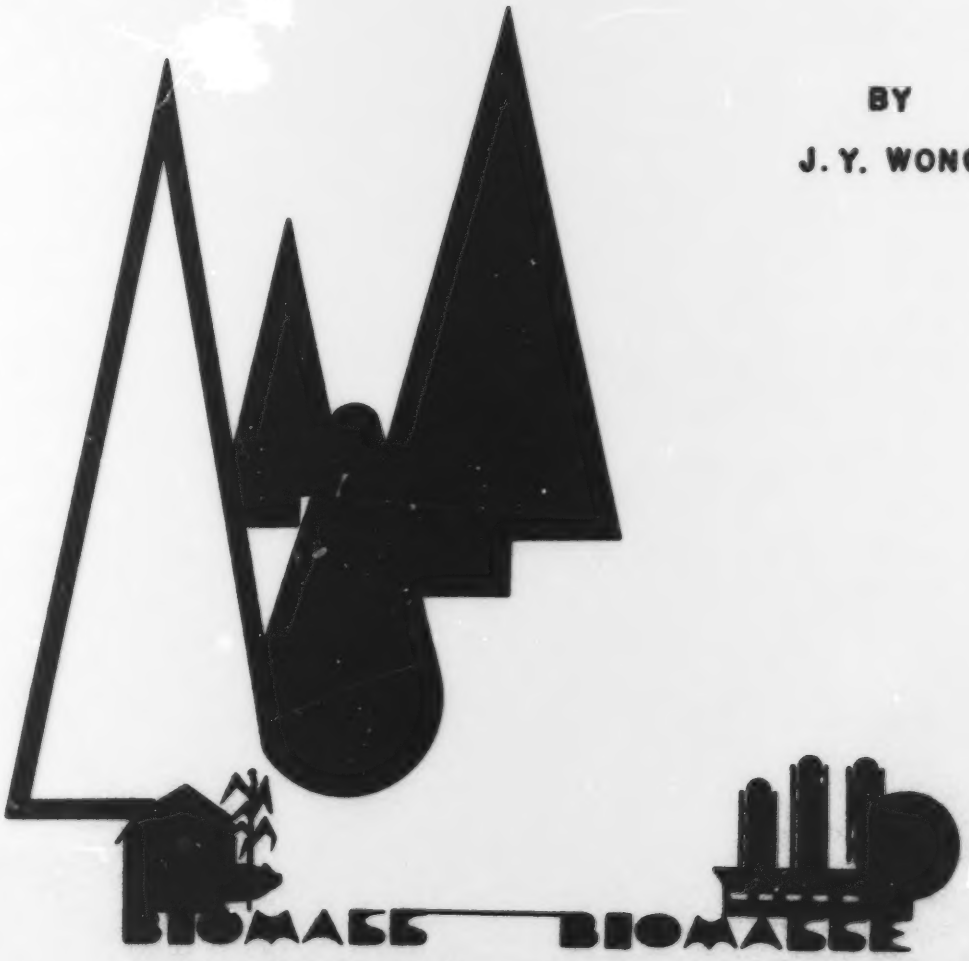

DIVISION OF ENERGY / DIVISION DE L'ÉNERGIE

Canada

NRCC 22961

85-3233/

This report summarizes work carried out under contract to the Division of Energy, National Research Council of Canada. It has been published in accordance with the policy of the National Research Council of Canada of making information on energy research and development available to all interested groups. Publication by the National Research Council of Canada does not signify that the contents necessarily reflect the views or policies of the National Research Council of Canada, nor does mention of trade names or commercial products constitute endorsement or recommendation for use. Furthermore, no warranty or representation is made with respect to the accuracy or completeness of the information contained in this report.

Le présent rapport constitue un résumé des travaux effectués à contrat par la Division de l'énergie, Conseil national de recherches du Canada (CNRC). Sa publication est conforme à la politique du CNRC qui est de diffuser l'information disponible sur la recherche et le développement énergétiques auprès de tous les groupes intéressés. Son contenu n'exprime pas nécessairement les opinions ou politiques du Conseil national de recherches du Canada et la mention de marques ou produits commerciaux ne doit pas être considérée comme une approbation ou une recommandation d'utilization. De plus, aucune garantie ni représentation ne peut être faite quant à l'exactitude ou à l'intégralité du contenu du rapport.

Copyright 1983 by
National Research Council of Canada

Permission is granted to quote short excerpts and to reproduce figures and tables from this report, provided that the source of such material is fully acknowledged.

Copies of this and other publications of the Division of Energy may be obtained by mailing the appropriate remittance (a Bank, Express, or Post Office Money Order, or a cheque made payable to the Receiver General for Canada, credit NRC) to

Publications Sales and Distribution Office
National Research Council of Canada
Ottawa, Ontario
K1A 0R6

Price: Free

Copyright 1983 par
Conseil national de recherches du Canada

De courtes citations et la reproduction de figures et tableaux du présent rapport sont autorisées sous réserve que la source en soit clairement mentionée.

Des exemplaires du rapport et d'autres publications de la Division de l'énergie peuvent être obtenus par courrier sur le paiement d'avance des droits requis (règlement par mandat de banque, mandat-exprès, mandat-poste ou cheque payables au Receveur général du Canada, crédit du CNRC) à l'adresse suivante:

Bureau de vente et diffusion des publications
Conseil national de recherches du Canada
Ottawa (Ontario)
K1A 0R6

Prix unitaire: Gratuit

EVALUATION OF SOIL STRENGTH MEASUREMENTS

J.Y. Wong

DECEMBER 1983

TABLE OF CONTENTS

	Page
FOREWORD	v
ABSTRACT/RÉSUMÉ	vii
NOMENCLATURE	ix
1. INTRODUCTION	1
2. DESCRIPTION OF TEST SITES	2
3. EQUIPMENT AND PROCEDURES FOR MEASURING THE MECHANICAL PROPERTIES OF THE TERRAIN	9
4. PRESSURE-SINKAGE TESTS	14
5. SHEAR TESTS	22
6. REPETITIVE LOADING TESTS	32
7. REMARKS	34
REFERENCES	34
APPENDIX A. KEY TO SOIL CLASSIFICATIONS	36
APPENDIX B. WET DENSITY, DRY DENSITY, AND MOISTURE CONTENT OF TEST AREAS	38

FOREWORD

This report has been prepared for the Bioenergy Program, Division of Energy, National Research Council of Canada. It details the results of an evaluation study of the strength of the terrain in two hybrid poplar plantation sites in Edwardsburg Township, Grenville County, near Prescott, Ontario. The measurements of the mechanical and physical properties of the terrain in the test sites were performed by the Mobility Study Group of the Transport Technology Research Laboratory, Carleton University. The members of the Group included: Dr. J.Y. Wong, Principal Investigator; J. Preston-Thomas, Senior Research Associate; and P. Preston-Thomas and G. Subramaniam, Research Assistants. The mechanical properties of the terrain were measured using a vehicle-mounted bevameter and analyzed on site using a portable automatic data processing system designed and built at Carleton. Field data were taken in April 1982.

Work described in this report owes much to discussions with Mr. T.B. Golob, Project Manager, of the National Research Council of Canada, and Dr. M.G. Bekker, Consultant, Santa Barbara, California. Assistance given by the Department of National Defence in providing a vehicle for mounting the bevameter and other equipment for field work is appreciated.

ABSTRACT

The pressure-sinkage relationships, shearing characteristics, and behaviour under repetitive loading of the terrain at two sites for poplar plantation in Grenville County, near Prescott, Ontario, have been measured and representative data have been obtained. From the data, the values of the parameters for characterizing the pressure-sinkage relationship and shear strength of the terrain have been derived.

RÉSUMÉ

On a mesuré les relations entre pression et enfoncement, les caractéristiques de cisaillement et le comportement du terrain sous l'effet de charges répétées en plus d'obtenir des données représentatives pour deux emplacements choisis pour la plantation de peupliers dans le comté de Grenville près de Prescott en Ontario. On a tiré de ces données les valeurs des paramètres caractérisant la relation entre pression et enfoncement et la résistance au cisaillement du terrain.

NOMENCLATURE

b	radius of a circular plate; width of a rectangular plate; smaller dimension of contact area
c	cohesion
j	shear displacement
j_0	shear displacement where maximum shear stress occurs
K	shear deformation modulus
K_r	ratio of the residual shear stress to the maximum shear stress
K_w	shear deformation modulus which is equivalent to j_0
k_c, k_ϕ	pressure-sinkage constants in the Bekker equation
k_c', k_ϕ'	pressure-sinkage constants in the Reece equation
n	exponent of terrain deformation
p	pressure
z	sinkage
τ	shear stress
τ_{max}	maximum shear stress
ϕ	angle of internal shearing resistance

EVALUATION OF SOIL STRENGTH MEASUREMENTS

J.Y. Wong

1. INTRODUCTION

In accordance with the Statement of Work of the contract entitled "Evaluation Study of Soil Strength Measurements", Serial Number OSX81-00132, the objectives of the work described in this report were

(a) to measure the pressure-sinkage relation, shear strength, moisture content, grain size distribution, and bulk density of the terrain under three different moisture conditions at two sites for poplar plantation in Grenville County, near Prescott, Ontario

(b) to analyze and evaluate the pressure-sinkage and shear test data obtained in the field, using computerized procedures as applicable

In accordance with the terms of the contract, the duration of field operations was limited to approximately three weeks. This limited the quantity of samples that could be taken in the test sites. While it is believed that the quantitative information derived from the samples is representative of the test areas, the data are not intended for comprehensive statistical analysis.

2. DESCRIPTION OF TEST SITES

The test sites are located on the south side of Lot 20, Concession II, in Edwardsburg Township, Grenville County, near Prescott, Ontario. The two test sites are shown on the attached map (Fig. 1). The site on the west side of the road is referred to as Site 1, whereas the one on the east side is referred to as Site 2. The approximate locations where terrain measurements were actually taken are identified by the numbered squares on the map. According to a soil survey map produced by the Department of Soils, Ontario Agricultural College, Guelph, and the Experimental Farms Service, Federal Department of Agriculture, Ottawa, the soil in areas 1-A, 1-B, 1-C, 1-D, and 1-E is classified as Upland sandy loam, the soil in area 2A is classified as Rubicon sandy loam, the soil in areas 2-B and 2-C is classified as North Gower clay loam, and that in area 2-D is classified as Grenville loam. The basic features of these soils as described in the soil survey map are reproduced for reference purposes in Appendix A.

According to the information provided by the Kemptville Office of the Ontario Ministry of Natural Resources, the test sites were prepared for planting in the summer and the fall of 1981. The bushes on the sites were first cleared and the roots were allowed to sprout. After spraying chemicals to eliminate the remaining living vegetation, the field was plowed to a depth of approximately 25 cm. This was followed by harrowing the field several times using disc harrows to a depth of approximately 15 to 20 cm.

Measurements of the mechanical properties of the terrain on the test sites commenced in the middle of April of 1982, approximately 10 days after the ground had thawed out. Soil samples were taken from the test areas and analyzed in the laboratory to determine the grain size distribution. Both the sieve and the hydrometer analysis methods were employed. Figures 2, 3, 4, and 5 show the grain size distribution for the soil samples taken in areas 1-A to 1-E, 2-A, 2-B and 2-C, and 2-D, respectively.

It should be mentioned that on the surface of some test areas, there was a fairly dense matrix of non-woody fibres (mainly dried out grass stems), as can be seen from Fig. 6. From the surface to a depth of approximately 30 cm, there were roots of woody shrubs in some test locations. The existence of non-woody fibres on the surface and the roots in the terrain should be borne in mind when interpreting the data on the bearing strength and shearing characteristics of the terrain.

The wet density, dry density, and moisture content of the terrain were measured using a Troxler Electronic Laboratories' Surface Moisture-Density Gauge, model 3411-B, shown in Fig. 6. The gauge was calibrated following the procedures given in the instruction manual. The readings of wet

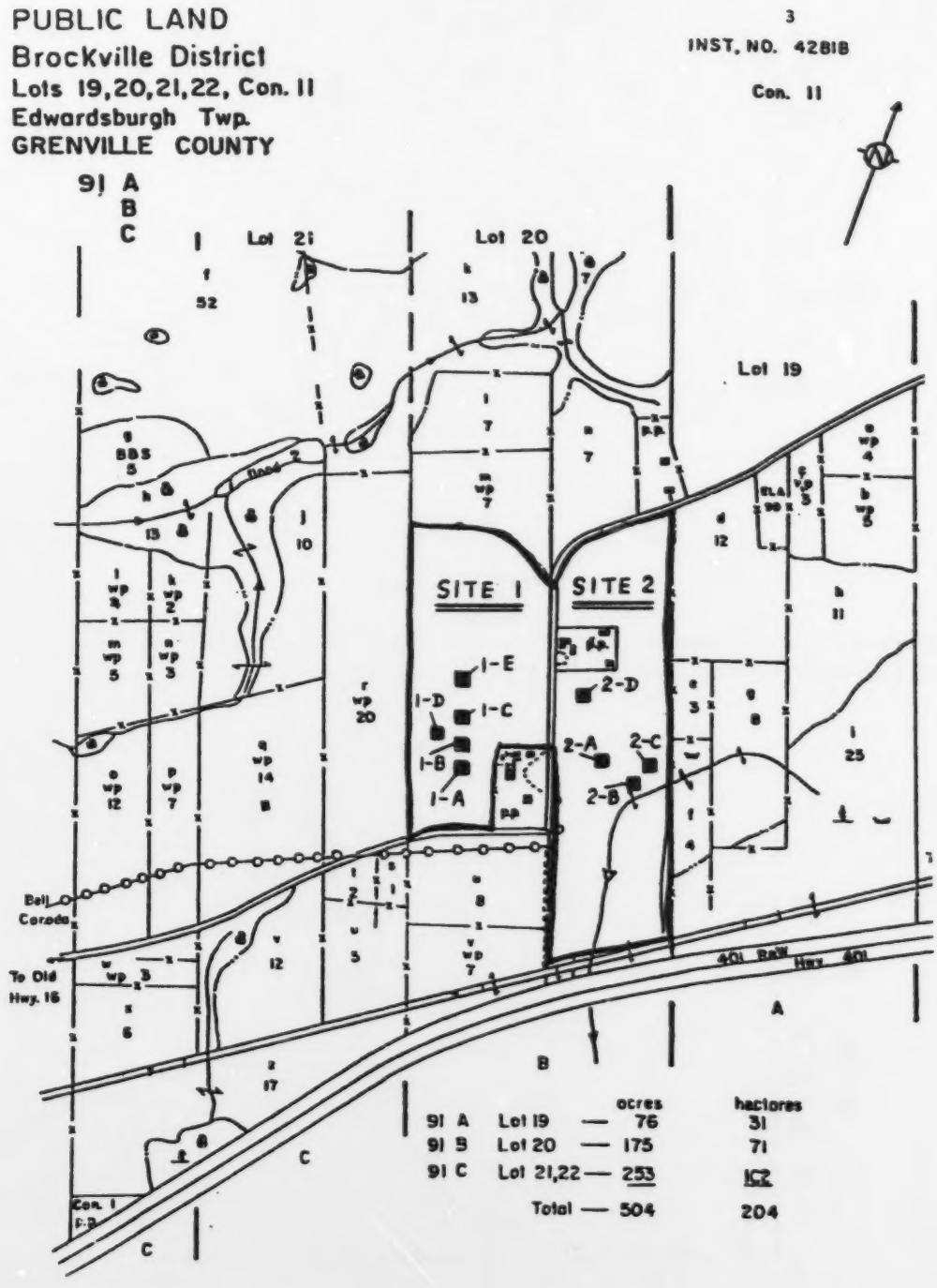

Figure 1. Map showing location of test sites

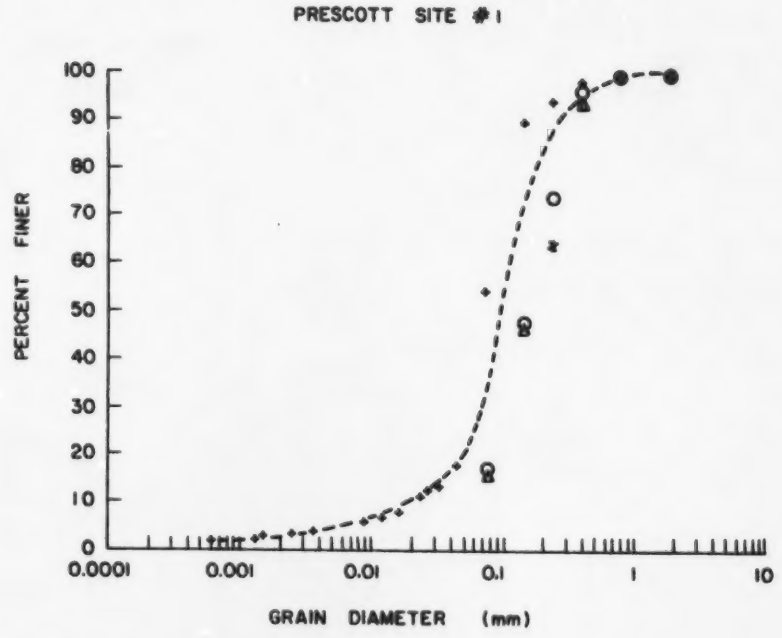

Figure 2. Grain size distribution for areas 1-A, 1-B, 1-C, 1-D, and 1-E in Site 1

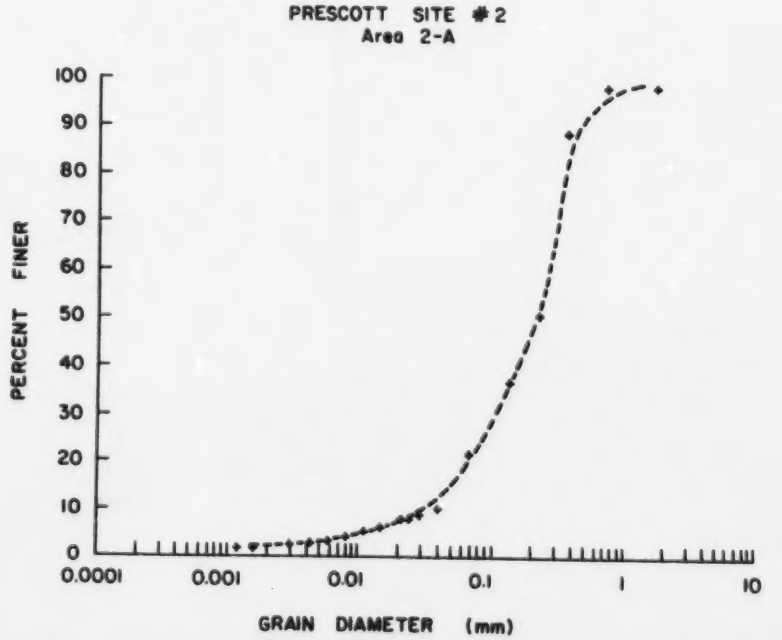

Figure 3. Grain size distribution for area 2-A in Site 2

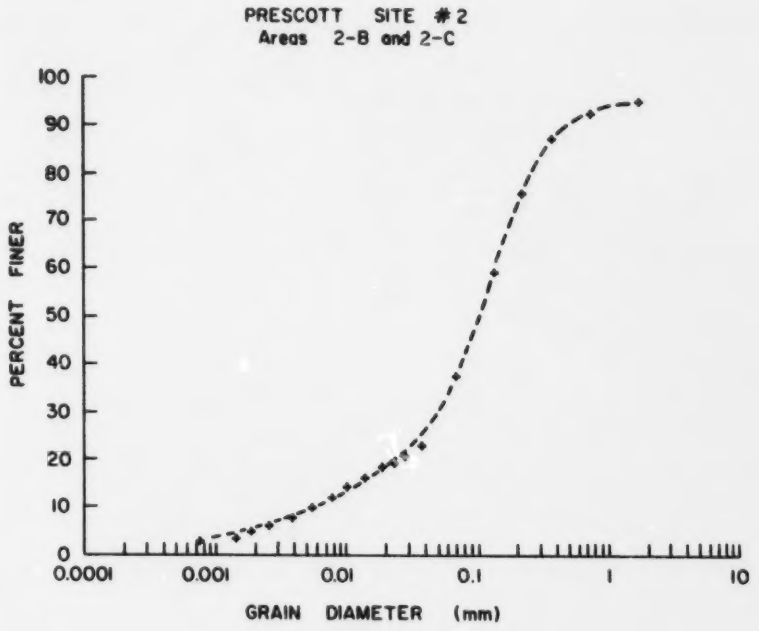

Figure 4. Grain size distribution for areas 2-B and 2-C in Site 2

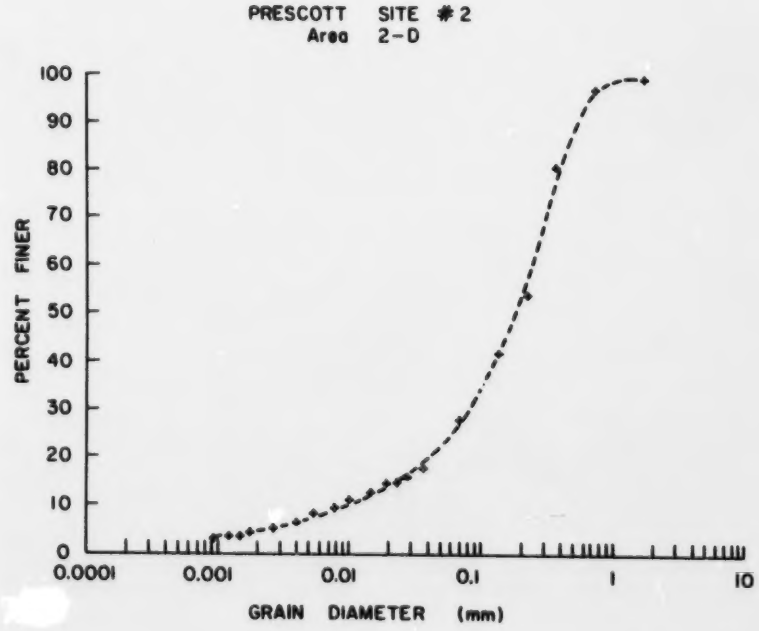

Figure 5. Grain size distribution for area 2-D in Site 2

Figure 6. Density and moisture gauge used in field testing

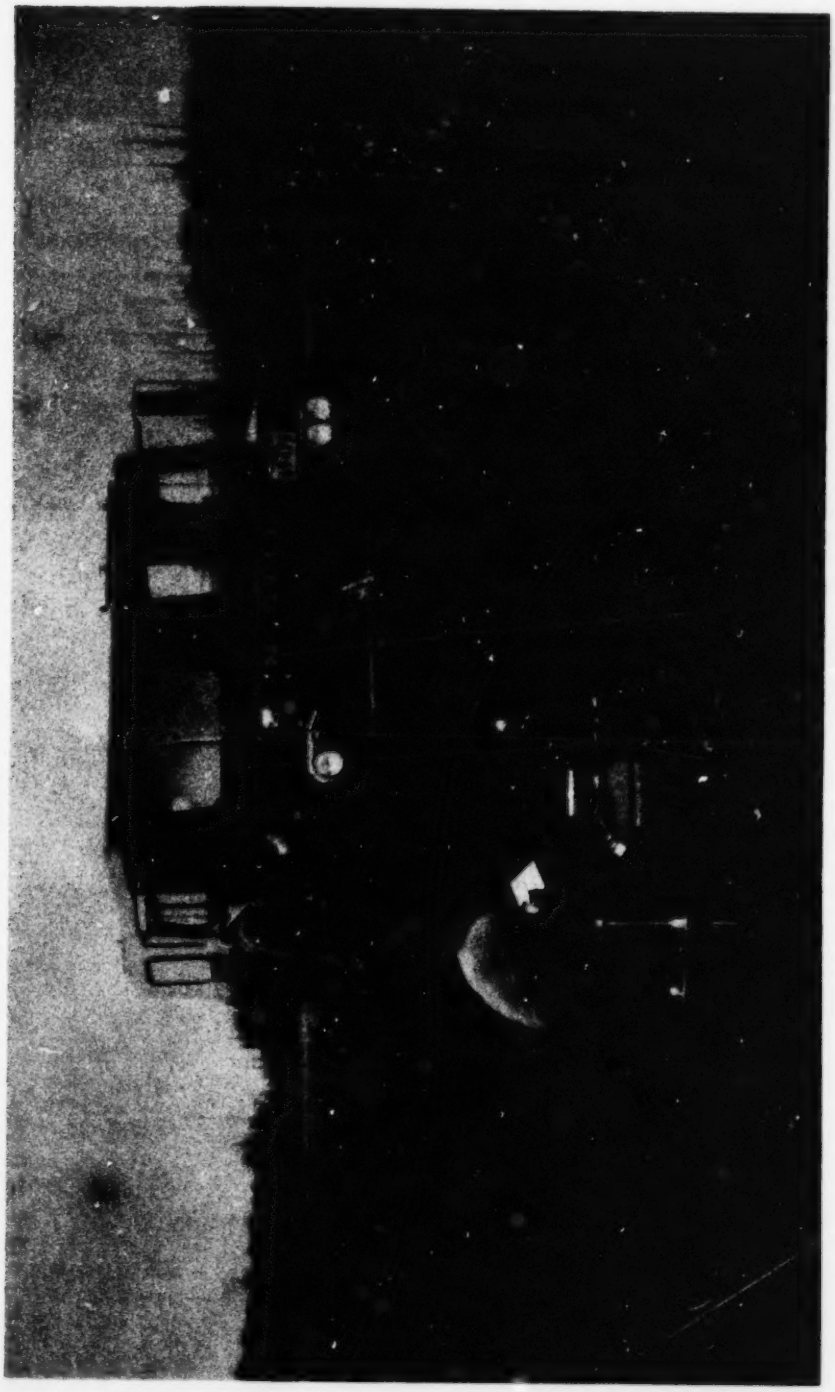

Figure 7. Bevameter and density and moisture gauge in operation

density, dry density, and moisture content obtained by the gauge were further checked by analyzing soil samples taken from the field. The wet density was determined by weighing the soil samples taken by a cylindrical sampler of 4.75 cm in diameter and 10 cm in height. The samples were then oven dried and the dry density and moisture content were determined. It was found that there was little difference between the readings taken by the gauge and those determined by the soil sampling technique. The readings of the wet density, dry density and moisture content at depths from 5 cm to 30 cm taken by the gauge at various test locations identified on the map are summarized in Appendix B. It should be pointed out that the density and moisture content measured by the gauge are the average values for the terrain between the surface and the depth indicated. This means, for instance, that the wet density indicated by the gauge at 30 cm represents the average value of wet density of the terrain between the surface and a depth of 30 cm. It should also be mentioned that the readings of density and moisture content of the terrain were taken at points as close as practicable to where the pressure-sinkage or shear tests were performed as shown in Fig. 7.

3. EQUIPMENT AND PROCEDURES FOR MEASURING THE MECHANICAL PROPERTIES OF THE TERRAIN

In accordance with the terms of the contract, the load-sinkage and shearing characteristics of the terrain were measured. In addition, to provide information for the evaluation of the multi-pass performance of vehicle running gear, the response of the terrain to repetitive loading was also measured. All the mechanical properties of the terrain were measured using a vehicle mounted bevameter, which has been successfully used since 1978 in measuring the mechanical properties of mineral terrain, muskeg, and snow (1-3). In the bevameter used, a hydraulic ram is mounted vertically at one end of the frame and is used to exert vertical loads on a sinkage plate during pressure-sinkage tests, as shown in Fig. 8. The shear head used in shear tests is mounted at the other end of the bevameter frame as shown in Fig. 9. It is driven by the hydraulic ram through a chain drive. The rate of loading (or shearing) can be adjusted using a flow control unit of the hydraulic system.

The load applied to the sinkage plate was monitored using a strain-gauge type load cell, Lebow-3132, with nominal load capacity of 15 kN (approximately 3000 lb). The load cell was calibrated in the laboratory prior to field tests. The sinkage (penetration) of the plate was measured with a calibrated potentiometer using the original surface of the terrain as a reference, as can be seen from Fig. 8. Circular plates of diameters of 7.5, 10, and 15 cm were used in pressure-sinkage and repetitive loading tests, and the rate of sinkage was kept at approximately 2.5 cm/s.

The torque applied to the shear head during shear tests was measured using a strain-gauge type torque sensor, Lebow 2110-2K with nominal load capacity of 226 N m (2000 lb in.). The torque sensor was calibrated in the laboratory prior to use in the field. The angular displacement of the shear head was monitored using a calibrated potentiometer. The shear ring used to measure the internal shearing characteristics of the terrain has an outside diameter of 34 cm, inside diameter of 27 cm, grouser height of 1 cm, and grouser spacing of 30°. To determine the characteristics of rubber-terrain shearing, a shear ring of the same outside and inside diameters, but covered with a layer of rubber about 3.5 mm thick (without grousers), was used.

To expedite the processing of the data collected by the bevameter, an automatic data processing system developed and built at the Transport Technology Research Laboratory, Carleton University, was used. The system has been successfully used in processing terrain data under field conditions since 1980 (3, 4). It was installed in the vehicle on which the bevameter was mounted. Figure 10 shows the system in operation inside the vehicle during field tests. The system was designed to process data

Figure 8. Pressure-sinkage tests using the bevameter

Figure 9. Shear tests using the bevameter

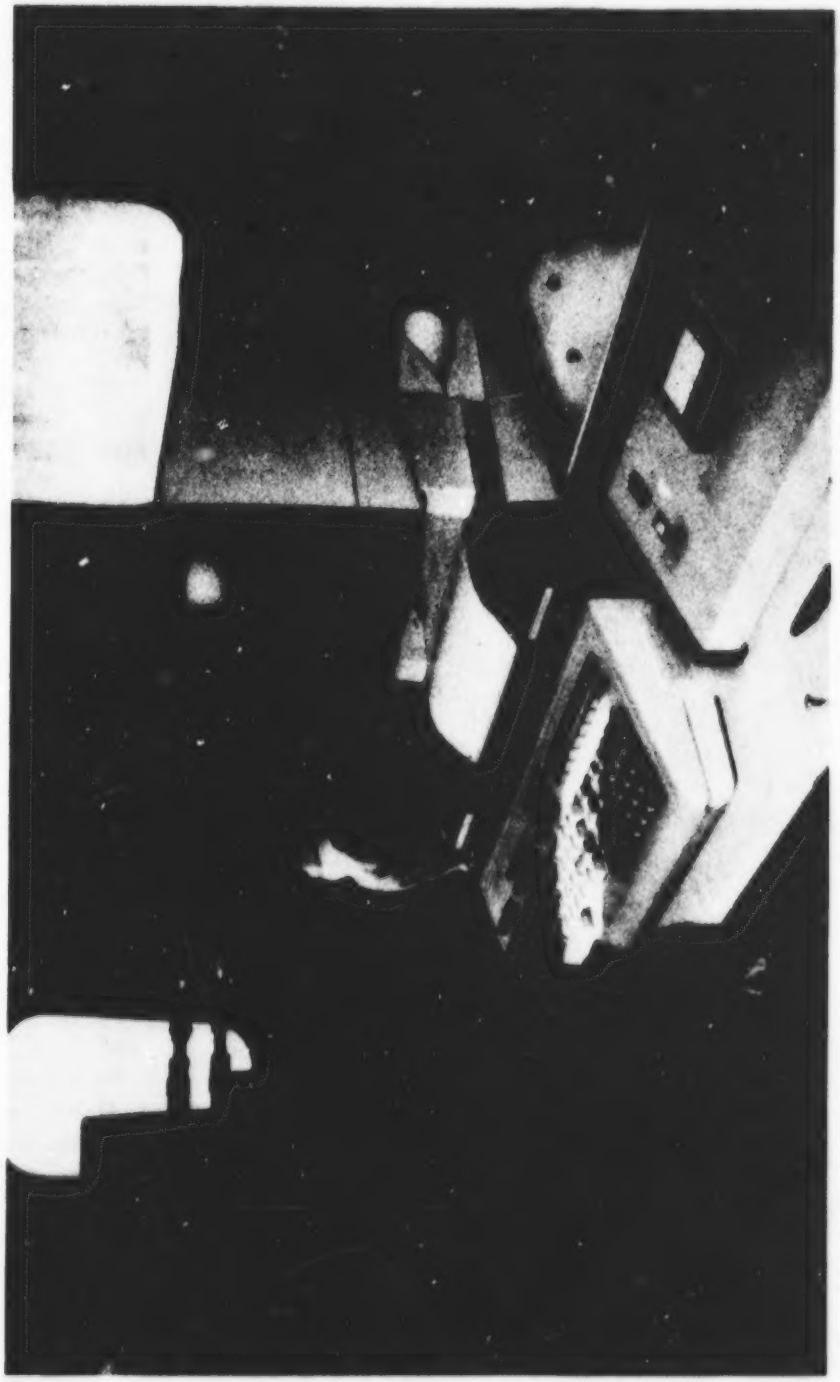

Figure 10. The automatic data processing system in operation

sampled by the bevameter and other similar devices. The test results together with the values of the parameters characterizing the behavior of the terrain are recorded with a thermal line printer immediately after each test and are also stored in cassette tapes for future reference. On completion of testing in a particular area the mean values of these parameters together with their standard deviations can also be printed out. The whole process is essentially automated and no manual treatment of the data is required. The block diagram of the data processing system is shown in Fig. 11 and the details of the design of the system can be found in reference 3.

Special software was developed to process the pressure-sinkage and shear test data on the microcomputer of the automatic data processing system. The details will be described in Sections 4 and 5 of this report.

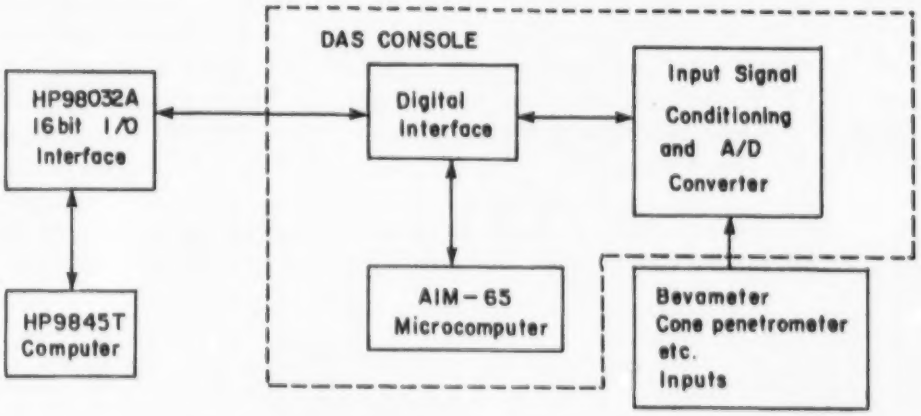

Figure 11. Block diagram for the automatic data processing system

4. PRESSURE-SINKAGE TESTS

During the pressure-sinkage test, the pressure and sinkage of the plate were monitored by the load cell and the potentiometer of the bevameter. The signals generated by the transducers were then transmitted to the automatic data processing system and the pressure-sinkage curve was plotted on the thermal printer. To minimize the effect of local variation of terrain conditions, the pressure-sinkage constants were not derived from individual pressure-sinkage curves. Instead, after completing a series of tests, usually two to five pairs, using two different sizes of plates, a mean pressure-sinkage curve for each of the two test plates was obtained. It should be mentioned that the distance between the points where two consecutive tests were performed was about 1 m. The mean curves were then fitted to both the Bekker and Reece pressure-sinkage equations. A weighted, least-squares method was employed to derive the pressure-sinkage constants from the mean curves. This procedure was computerized and a package of special software was developed for analyzing the data. The details of the procedure based on the weighted, least-squares principle have been described previously (2). However, some of the basic features are briefly reviewed below.

Consider the pressure-sinkage equation proposed by Bekker as an example. Taking the logarithms of both sides of the following equation,

$$[1] \qquad p = (k_c/b + k_\phi)z^n$$

one obtains

$$[2] \qquad \ln p = \ln (k_c/b + k_\phi) + n \ln z$$

In Eq. [2], p and z are measured values and b is the width (or radius) of the plate. k_c, k_ϕ, and n are constants to be determined from experimental data. To obtain the best fitting line, based on Eq. [2], the conventional least-squares technique cannot be directly employed, as p and z are the measured quantities, not ln p and ln z. Applying the conventional least-squares principle to the logarithms of the deviations will give excessive weight to deviations at low pressures, which are usually the least significant. However, one may approach the problem by introducing a weighting factor and by minimizing the value of

$$[3] \qquad w_r[\ln p - \ln (k_c/b + k_\phi) - n \ln z]^2$$

where w_r is an appropriate weighting factor.

If an equal liability to error for all observations is assumed, the weighting factor w_r may be taken as

[4] $$w_r = p^2$$

Thus to obtain the best values of k_c, k_ϕ, and n for a particular set of test data, the following function must be minimized

$$F = \sum p^2[\ln p - \ln (k_c/b + k_\phi) - n \ln z]^2$$

or

[5] $$F = \sum p^2[\ln p - \ln k_{eq} - n \ln z]^2$$

where

$$k_{eq} = k_c/b + k_\phi$$

To minimize the value of the function F, the first partial derivatives of F with respect to n and to k_{eq} are taken and set to zero. This leads to the following two equations:

[6] $$\ln k_{eq} \sum p^2 \ln z + n \sum p^2 (\ln z)^2 = \sum p^2 \ln p \ln z$$

[7] $$\ln k_{eq} \sum p^2 + n \sum p^2 \ln z = \sum p^2 \ln p$$

Solving these two equations simultaneously, one can obtain the best fitting values of n and $\ln k_{eq}$ for a particular set of data

[8] $$n = \frac{\sum p^2 \sum p^2 \ln p \ln z - \sum p^2 \ln p \sum p^2 \ln z}{\sum p^2 \sum p^2 (\ln z)^2 - (\sum p^2 \ln z)^2}$$

[9] $$\ln k_{eq} = \frac{\sum p^2 \ln p - n \sum p^2 \ln z}{\sum p^2}$$

It should be mentioned that in practice the values of n calculated from the two sets of data obtained using two different sizes of plates are seldom identical, even under controlled laboratory conditions. Since the Bekker equation implies that for a particular type of terrain there is a unique value of n, an average value, n_{av}, is taken

[10] $$n_{av} = \frac{(n)_{b=b_1} + (n)_{b=b_2}}{2}$$

where $(n)_{b=b_1}$ and $(n)_{b=b_2}$ represent the values of n obtained from the two sets of data using plates with widths b_1 and b_2, respectively.

The value of n_{av} is then used to recalculate the value of k_{eq} for a particular set of data

$$[11] \qquad \ln k_{eq} = \frac{\sum p^2 \ln p - n_{av} \sum p^2 \ln z}{\sum p^2}$$

From the two sets of test data, two values for k_{eq}, one from the data obtained using a plate with width b_1, $(k_{eq})_{b=b_1}$, and the other from the data obtained using a plate with width b_2, $(k_{eq})_{b=b_2}$, can be derived. Thus the values of k_c and k_ϕ can be calculated by

$$[12] \qquad k_c = \frac{(k_{eq})_{b=b_1} - (k_{eq})_{b=b_2}}{b_2 - b_1} b_1 b_2$$

$$[13] \qquad k_\phi = (k_{eq})_{b=b_1} - \frac{(k_{eq})_{b=b_1} - (k_{eq})_{b=b_2}}{b_2 - b_1} b_2$$

The above procedures have been computerized and incorporated into the automatic data processing system. Upon completion of a set of tests, values of k_c, k_ϕ, and n are printed on paper as outputs of the data processing system.

To evaluate the goodness-of-fit using the above procedures, the ratio of the r.m.s. error to the mean value of presure is calculated

$$[14] \qquad \varepsilon = 1 - \frac{\left\{ \frac{[\sum (p_m - p_c)^2]}{(N - 2)} \right\}^{1/2}}{\sum p_m / N}$$

where p_m is the measured pressure, p_c is the calculated pressure using the procedures described above, and N is the number of data points used for the curve fitting. When $\varepsilon = 1$, the fit is perfect. The calculation of ε for each set of data is computerized and its value is printed out.

An approach similar to that described above may be followed to fit the pressure-sinkage data to the Reece equation. From the curve-fitting point of view, the original Reece's equation can be rewritten as

$$[15] \qquad p = (k_c' + bk_\phi')(z/b)^n$$

where n, k_c', and k_ϕ' are pressure-sinkage constants.

Employing the weighted, least-squares method described previously, one obtains the best fitting values of n and k_{eq}' (which is equal to $k_c' + bk_\phi'$) for a particular set of experimental data

$$[16] \qquad n = \frac{\sum p^2 \sum p^2 \ln p \ln (z/b) - \sum p^2 \ln p \sum p^2 \ln (z/b)}{\sum p^2 \sum p^2 (\ln z/b)^2 - [\sum p^2 \ln (z/b)]^2}$$

$$[17] \qquad \ln k'_{eq} = \frac{\sum p^2 \ln p - n \sum p^2 \ln (z/b)}{\sum p^2}$$

As pointed out previously, the values of n calculated from the two sets of data obtained using two different sizes of plates are seldom identical. Therefore, an average value, n_{av}, is taken

$$[18] \qquad n_{av} = \frac{(n)_{b=b_1} + (n)_{b=b_2}}{2}$$

This value is then used to obtain the value of k'_{eq} for a particular set of data

$$[19] \qquad \ln k'_{eq} = \frac{\sum p^2 \ln p - n_{av} \sum p^2 \ln (z/b)}{\sum p^2}$$

From two sets of test data, two values of k'_{eq}, one from the data obtained using a plate with width b_1, $(k'_{eq})_{b=b_1}$, and the other from the data obtained using a plate of width b_2, $(k'_{eq})_{b=b_2}$, can be derived. Thus the values of k'_c and k'_ϕ can be calculated by

$$[20] \qquad k'_c = (k'_{eq})_{b=b_1} - \frac{[(k'_{eq})_{b=b_1} - (k'_{eq})_{b=b_2}]}{b_1 - b_2} b_1$$

$$[21] \qquad k'_\phi = \frac{[(k'_{eq})_{b=b_1} - (k'_{eq})_{b=b_2}]}{b_1 - b_2}$$

This procedure for fitting pressure-sinkage data with the Reece equation has been computerized and incorporated into the automatic data processing system. The values of n, k'_c, and k'_ϕ are printed on paper as outputs of the data processing system.

It is interesting to point out that fitting the same set of load-sinkage data with either the Bekker or the Reece equation results in the same goodness-of-fit. Furthermore, the values of n in both cases are identical. This is because the value of b (the width or the radius of the plate) is a constant for a particular set of data. Consequently both the Bekker and the Reece equations are of similar form. The curves calculated

from both the Bekker and the Reece equations, therefore, collapse to a single curve. This does not mean, however, that the Bekker and the Reece equations will give the same prediction of pressure for any particular loading plate at any specific sinkage.

Figure 12 shows a representative computer printout, on which the best-fitted curve to a set of pressure-sinkage curves obtained experimentally is plotted and the associated pressure-sinkage constants are given. The

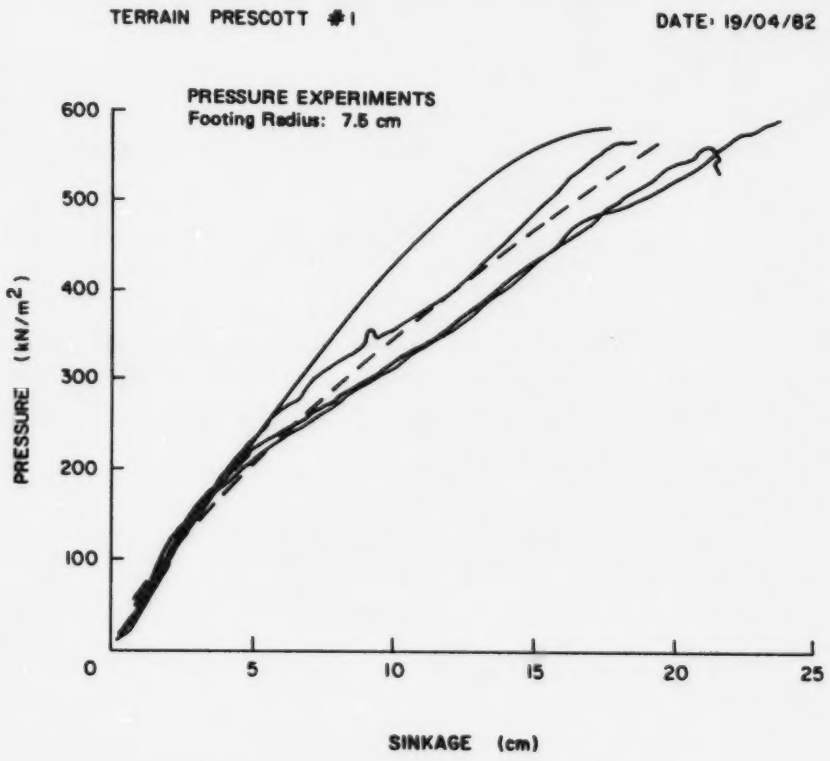

Figure 12. Pressure-sinkage test results. Average values for the set are

	Bekker	Reece
N_{av}	737.1E-03	737.1E-03
K_ϕ	152.2E+01 (kN/m^{n+2})	209.2E+01 (kN/m^3)
K_c	268.4E-01 (kN/m^{n+1})	121.7E+00 (kN/m^2)

The goodness-of-fit of the data to each of the Bekker and Reece equations is 95.1%

goodness-of-fit, as defined by Eq. [14], of the mean curve to the Bekker and Reece equations is also given.

As mentioned in Section 2, the test sites were plowed and then harrowed to a depth of 15 to 20 cm in the previous summer and fall. This indicates that the terrain is expected to be stratified and consequently the pressure-sinkage relationship is expected to have a noticeable change at a depth between 15 and 20 cm. This has been well borne out in many cases by the measured pressure-sinkage curves. Furthermore, observations of the operation of the two test tractors (a Versatile and a Holder four-wheel drive tractor) in the field showed that the depth of the ruts made by the tires did not exceed 20 cm. To provide appropriate terrain data for the prediction and evaluation of these two test vehicles, which is one of the objectives of this work, the measured pressure-sinkage curves were fitted to the equations up to a depth of 20 cm. The pressure-sinkage constants, that is, n, k_ϕ, and k_c in the Bekker equation and n, k'_ϕ and k'_c in the Reece equation, shown in Fig. 12, are therefore appropriate for sinkages up to 20 cm.

Tables 1 and 2 summarize the results of the pressure-sinkage tests. The first column in the tables identifies the date and the test area, shown on the map in Section 2 (Fig. 1). The values of the pressure-sinkage constants for a particular test area for sinkages up to 20 cm are then listed. The reference number given in the tables refers to the identification number of the data sets of terrain density and moisture content given in Appendix B. The wet density, dry density, and moisture content shown in the tables correspond to the mean values obtained from the data sets, identified by the reference number, at a depth of 20 cm.

It should be pointed out that when comparing the bearing strength of different terrains, one should consider the values of the three pressure-sinkage constants (n, k_ϕ, and k_c for the Bekker equation, and n, k'_ϕ, and k'_c for the Reece equation) as a whole. The value of the exponent n or the values of k_ϕ and k_c (or k'_ϕ and k'_c) alone cannot be used as a sole indicator of the firmness of a terrain. For example, if two types of terrain have the same values of k_ϕ and k_c, but one has a higher value of n than the other, then for the same size of plate at the same sinkage of, say, 0.2 m, the reaction exerted on the plate by the terrain having a higher value of n will be less than that of the other. This means that under these circumstances, the terrain having a higher value of n is softer than that having a lower value of n. Furthermore, for a given terrain, the value of k_ϕ (or k'_ϕ) is associated with a particular value of k_c (or k'_c). They should be considered together as a group and not separately.

Table 1. Summary of pressure-sinkage constants - Prescott Site #1

Date (Area)	n	k_ϕ (kN/m^{n+2})	k_c (kN/m^{n+1})	k'_ϕ (kN/m^2)	k'_c (kN/m^2)	Ref. no.	Wet density (kg/m^3)	Dry density (kg/m^3)	Moisture content (%)
Apr. 16						16-1			
(1-A)	1.10	2080	74.6	1833	42.0	16-2	1557	1028	51.6
						16-3			
	0.97	1418	65.5	1464	77.4	16-4	1542	1033	49.2
						16-5			
	1.00	2293	5.7	2283	5.3	16-5	1570	1053	49.1
						16-6			
Apr. 19	0.74	1522	26.8	2092	121.7	19-7	1519	1053	44.3
(1-B)						19-8			
Apr. 22						22-1			
(1-C)	1.74	1643	259.0	763	-0.9	22-2	1696	1131	50.0
						22-3			
Apr. 23	0.85	2529	3.3	3270	42.4	23-1	1471	1144	28.6
(1-D)	0.72	1856	59.1	2323	231.4	23-2	1592	1185	34.3
	0.77	2761	58.4	3626	214.1	23-3	1559	1153	35.1
	1.09	3573	24.9	2982	6.7	23-5	1716	1307	31.2
						26-1			
Apr. 26	0.70	1426	70.6	1317	279.3	26-2	1470	1152	27.3
						26-3			
(1-E)	0.75	2464	55.7	3244	213.6	26-4	1526	1155	32.6
						26-5			

Density and moisture data for depth of 28 cm.

Table 2. Summary of pressure-sinkage constants - Prescott Site #2

Date (Area)	n	k_ϕ (kN/m^{n+1})	k_c (kN/m^{n+2})	k'_ϕ (kN/m^2)	k'_c (kN/m^2)	Ref. no.	Wet density (kg/m^3)	Dry density (kg/m^3)	Moisture content (%)
Apr. 27	0.66	752	6.9	1176	63.3	27-1	1561	1091	43.3
(2-A)	0.65	880	10.5	1358	88.2	27-3	1588	1100	44.2
						27-4			
Apr. 28	0.73	2471	41.6	-4.2	121.2	28-1	1681	1100	45.8
(2-B)						28-2			
Apr. 29	0.85	1134	6.8	1430	27.0	29-4	1597	1053	52.0
(2-C)						29-5			
Apr. 30	1.01	5880	0.06	5814	-1.3	30-1	1326	1069	24.1
(2-D)						30-2			
	1.02	4486	66.0	4292	55.3	30-3	1339	1133	18.2

Density and moisture data for depth of 28 cm.

5. SHEAR TESTS

A series of shear tests with various normal loads was performed on different test areas. During the shear test, the torque applied to the shear head and its angular displacement were monitored by the torque sensor and the potentiometer of the bevameter. The signals from the transducers were then transmitted to the automatic data processing system and the torque-shear displacement curve was plotted on the thermal printer. After completing a series of tests with a number of normal loads, usually 5 to 7, the shear strength parameters, cohesion (or adhesion) c and angle of shearing resistance ϕ, were determined and printed out.

To provide input data for predicting and evaluating the thrust-slip characteristics of off-road vehicles, the shear stress-displacement relation has to be characterized. The mathematical modelling of the shear stress-displacement relationship has attracted considerable interest of researchers in land locomotion mechanics. Some of the models that have been used previously are briefly reviewed here and a new model for the type of shear stress-displacement curves obtained at the test sites is proposed.

For "brittle" soils which display a "hump" of maximum shear stress, Bekker proposed the following equation (5, 6).

$$[22] \qquad \frac{\tau}{\tau_{max}} = \frac{\exp\left\{[-K_2 + (K_2^2 - 1)^{1/2}]K_1 j\right\} - \exp\left\{[-K_2 - (K_2^2 - 1)^{1/2}]K_1 j\right\}}{\exp\left\{[-K_2 + (K_2^2 - 1)^{1/2}]K_1 j_0\right\} - \exp\left\{[-K_2 - (K_2^2 - 1)^{1/2}]K_1 j_0\right\}}$$

where τ and τ_{max} are shear stress and maximum shear stress, respectively; j and j_0 are the shear displacement and the shear displacement at τ_{max}, respectively; K_1 and K_2 are constants. Various methods have been proposed for deriving the values of K_1 and K_2 from experimentally determined shear curves, such as those suggested by Weiss and Sela (6). Usually the deriving of the values of K_1 and K_2 from experimental shear curves is a very involved process, and as pointed out by Bekker, "accurate definitions of K_1 and K_2 values are difficult without computer methods" (6). It should be mentioned that Eq. [22] is identical in form to the curve describing an aperiodic motion of an overdamped, single-degree-of-freedom vibrating system in free vibration. Thus, when $j >> j_0$, τ/τ_{max} approaches zero.

For "plastic" soils which do not exhibit a "hump" of maximum shear stress, a simpler equation of the following form containing only one constant has been widely used.

$$[23] \qquad \frac{\tau}{\tau_{max}} = 1 - \exp(-j/K)$$

where K is a constant. It is a measure of the magnitude of the shear deformation required to develop the maximum shear stress.

It has been found that for certain types of fresh snow, peat, and sand, and for rubber-snow, rubber-muskeg mat, rubber-peat, and rubber-sand shearing, the shear stress-displacement relationship can be fairly well described by Eq. [23] (see references 1 to 3).

For the internal shearing of muskeg mat, it has been found that the shear curves fit the following equation fairly well (1, 3).

$$[24] \qquad \frac{\tau}{\tau_{max}} = (j/K_w) \exp (1-j/K_w)$$

where K_w is a constant. In physical terms, K_w is equal to the shear displacement j_0 where the shear stress peaks.

It has been found, however, that the shear curves obtained in the two test sites cannot fit to either Eq. [23] or Eq. [24] with sufficiently high accuracy. A typical shear curve obtained from the test sites displays a "hump" of maximum shear stress at a certain shear displacement j_0. Beyond the shear displacement j_0, the shear stress decreases and approaches a more or less constant level of residual stress as shown in Fig. 13. Inspired by the work of Pokrovski and of Kacigin and Guskov, Oida proposed the following equation to describe this type of shear stress-displacement curve (7, 8).

$$[25] \qquad \frac{\tau}{\tau_{max}} = K_r \left(1 - \frac{(1 - K_r)^{1/2}\{1 + [(1 - K_r)^{1/2} - 1]/K_r\}^{j/K_w}}{(1 - K_r)^{1/2}(1 - 2/K_r) + 2/K_r - 2}\right) \times \left(1 - \{1 + [(1 - K_r)^{1/2} - 1]/K_r\}^{j/K_w}\right)$$

where K_r is the ratio of the residual shear stress τ_r to the maximum shear stress τ_{max}, and K_w is the shear displacement where τ_{max} occurs (i.e., $K_w = j_0$).

An analysis of Eq. [25] shows that it satisfies the following conditions:

a. when $j = K_w$, $\tau = \tau_{max}$

b. when $j = K_w$, $d\tau/dj = 0$

c. when $j >> K_w$, $\tau \to \tau_r$

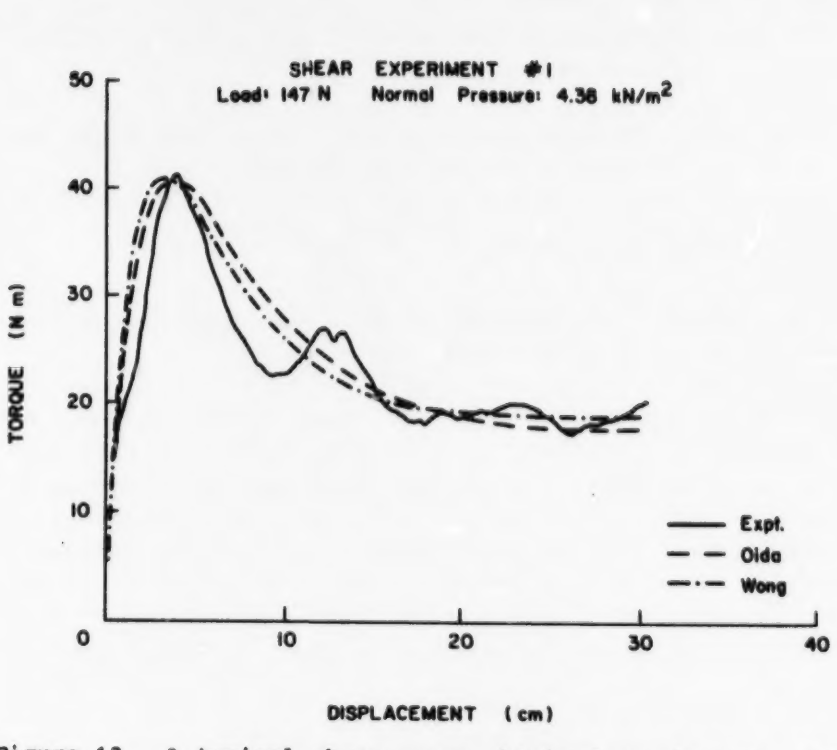

Figure 13. A typical shear curve obtained at the test site

	Oida	Wong
K_r	0.431	0.462
Goodness-of-fit (%)	85.1	85.5

Figure 14 shows the relationship between τ/τ_{max} and j/K_w at various values of K_r based on Eq. [25]. One of the major differences between Eq. [22] and Eq. [25] is that when $j >> j_0$, τ approaches zero using Eq. [22], whereas using Eq. [25], when $j >> K$, τ approaches τ_r.

Although Eq. [25] has certain attractive features, it is relatively complex. Furthermore, in most cases experimental shear curves do not exactly fit Eq. [25]. To minimize the error in curve fitting, an optimization procedure, for instance, has to be introduced to derive an optimum value of K_r. Owing to the nonlinear nature of the relation between τ/τ_{max} and K_r, the procedure for obtaining an optimum value of K_r for a

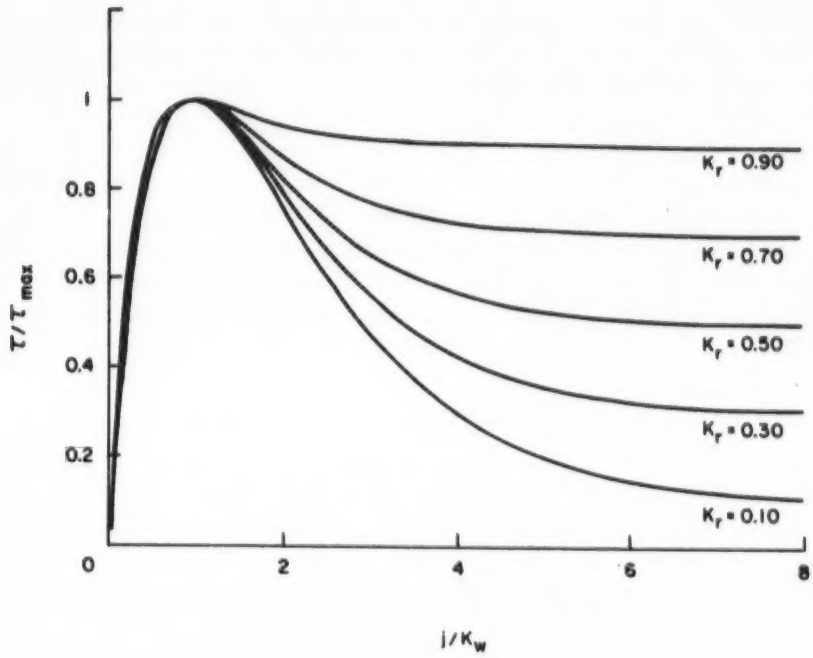

Figure 14. Variation of shear stress ratio τ/τ_{max} with shear displacement r ratio j/K_w for the Oida equation

particular experimental shear curve is relatively complex and time consuming.

In an attempt to overcome some of the drawbacks of Eq. [25], the following equation, which, similar to Oida's equation, originates from Pokrovski's work, is suggested by Wong.

$$[26] \quad \frac{\tau}{\tau_{max}} = K_r\left(1 + \left\{1/[K_r(1 - 1/e)] - 1\right\} \exp\,(1 - j/K_w)\right)[1 - \exp\,(-j/K_w)]$$

where K_w is the shear displacement where τ_{max} occurs ($K_w = j_0$).

Equation [26] satisfies the conditions that when $j = K_w$, $\tau = \tau_{max}$; and when $j >> K_w$, τ approaches τ_r. However, it can only satisfy the condition that $j = K_w$, $d\tau/dj = 0$, when $K_r = 0.662$. This means that when $K_r \neq 0.662$, the value of the maximum shear stress predicted using Eq. [26] will be slightly different from that obtained from experiment. However, the difference in most cases ($0.3 < K_r < 0.9$) is less than 3%. It should also be pointed out that the maximum shear stress predicted using Eq. [26] occurs at a shear displacement slightly different from K_w obtained from

experiment, if $K_r \neq 0.662$. The relationship between τ/τ_{max} and j/K_w at various values of K_r based on Eq. [26] is illustrated in Fig. 15. In spite of these, it has been found that Eq. [26] still gives fairly good fit to experimental shear curves obtained in the field, which will be shown later.

The procedure for deriving the optimum value of K_r that minimizes the error in fitting experimental shear curves to Eq. [26] is much simpler than that using Eq. [25]. Following the least-squares principle, to obtain the optimum value of K_r of Eq. [26] for a particular shear curve, the following function, which represents the sum of the square of the deviations, should be minimized

$$[27] \qquad F = \sum\left(\frac{\tau}{\tau_{max}} - K_r\left[1 + \left\{1/[K_r(1 - 1/e)] - 1\right\} \exp\,(1 - j/K_w)\right] \times [1 - \exp\,(-j/K_w)]\right)^2$$

To minimize the value of the function F, the first partial derivative of F with respect to K_r is taken and set to zero. This leads to the following expression for determining the optimum value of K_r for a particular set of shear test data.

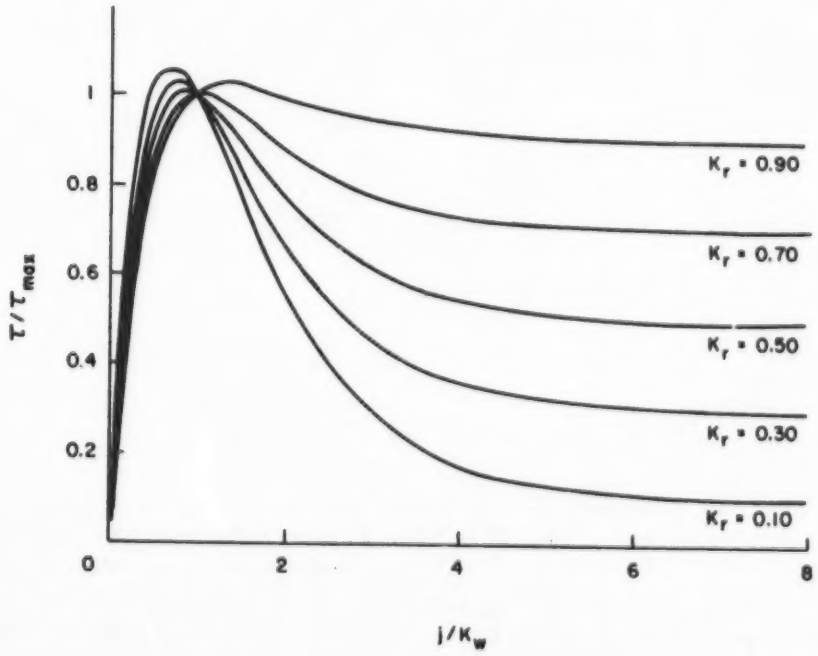

Figure 15. Variation of shear stress ratio τ/τ_{max} with shear displacement ratio j/K_w for the Wong equation

$$[28] \qquad K_r = \{\sum \frac{\tau}{\tau_{max}}[1 - \exp(1 - j/K_w)][1 - \exp(-j/K_w)]$$

$$- \sum \frac{1}{(1 - 1/e)}[1 - \exp(1 - j/K_w)][1 - \exp(-j/K_w)]^2$$

$$\times \exp(1 - j/K_w)\}/\{\sum[1 - \exp(1 - j/K_w)]^2[1 - \exp(-j/K_w)]^2\}$$

It has been found that the computing time required for obtaining the optimum value of K_r for a particular shear curve using Eq. [26] is an order of magnitude shorter than that using Eq. [25]. This is a significant advantage when data processing is being carried out on site.

Figure 16 shows a comparison between the fitted curves using Eqs. [25] and [26] for a particular set of shear data obtained in the field. It can be seen that there is little difference in the goodness-of-fit using Eq. [25] and Eq. [26]. In fact, for the particular case shown, Eq. [26] gives a better fit than Eq. [25], as evidenced from the values of goodness-of-fit (86.8% against 85.4% in Fig. 16).

It is interesting to point out that Eqs. [23], [24], and [26] belong to the same family of exponential functions. In fact, Eqs. [23] and [24] may be regarded as special forms of Eq. [26], since it contains exponential terms of $\exp(1 - j/K_w)$ and $[1 - \exp(-j/K_w)]$.

Based on a considerable amount of field experience, the following practical suggestions are made regarding the modelling of shear curves:

(a) If a shear curve does not display a "hump" of maximum shear stress and the shear stress increases with shear displacement continuously but approaches a constant value, then Eq. [23] may be used

$$\frac{\tau}{\tau_{max}} = 1 - \exp(-j/K)$$

The optimum value of K that minimizes the error in curve fitting is determined by (1, 2)

$$[29] \qquad K = -\frac{\sum(1 - \tau/\tau_{max})^2 j^2}{\sum(1 - \tau/\tau_{max})^2 j[\ln(1 - \tau/\tau_{max})]}$$

(b) If a shear curve exhibits a "hump" of maximum shear stress and then the shear stress decreases continually, such as that observed in the shearing of muskeg mat, then Eq. [24] may be used (1, 2)

$$\frac{\tau}{\tau_{max}} = (j/K_w) \exp(1 - j/K_w)$$

TERRAIN: PRESCOTT #1 DATE: 26/04/82

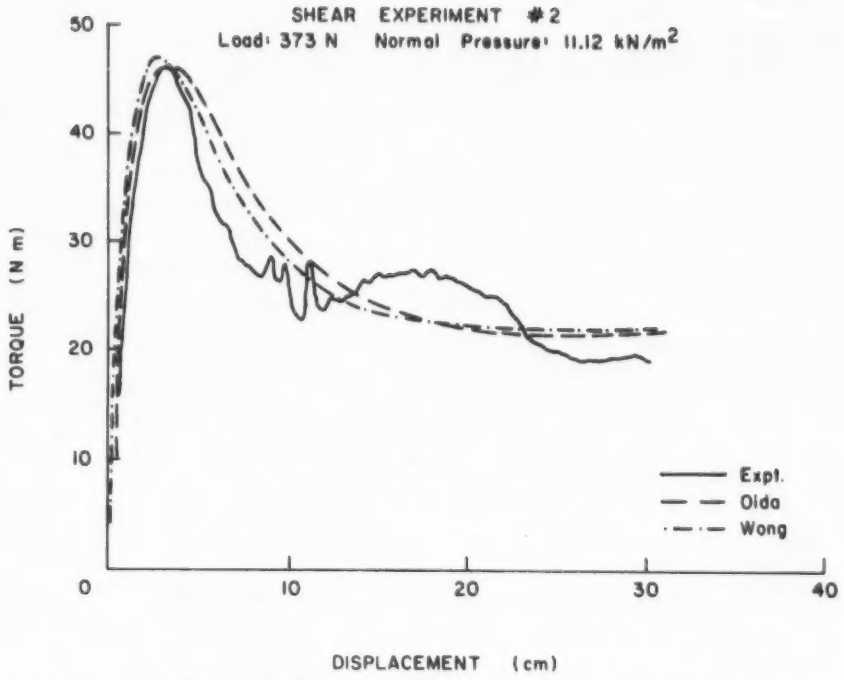

Figure 16. Goodness-of-fit to a shear curve using the Oida and the Wong equations

	Oida	Wong
K_r	0.462	0.475
Goodness-of-fit (%)	85.4	86.8

The optimum value of K_w that minimizes the error in curve fitting can be derived from solving the following equation

$$[30] \quad \sum (\tau/\tau_{max})^2 [\ln (\tau/\tau_{max}) - (1 + \ln (j/K_w) - j/K_w)][K_w - j] = 0$$

Usually an iteration procedure has to be employed to solve for K_w from Eq. [30].

(c) If a shear curve displays a "hump" of maximum shear stress and

then the shear stress decreases and approaches a constant value of residual shear stress, then Eq. [26] may be used:

$$\frac{\tau}{\tau_{max}} = K_r\{1 + \{1/[K_r(1 - 1/e)] - 1\} \exp (1 - j/K_w)) [1 - \exp (-j/K_w)]$$

The optimum value of K_r that minimizes the error in curve fitting is determined by

$$K_r = \{\sum \frac{\tau}{\tau_{max}} [1 - \exp (1 - j/K_w)][1 - \exp (-j/K_w)]$$

$$- \sum \frac{1}{(1 - 1/e)} [1 - \exp (1 - j/K_w)][1 - \exp (-j/K_w)]^2$$

$$\times \exp (1 - j/K_w)\}/\{\sum [1 - \exp (1 - j/K_w)]^2 [1 - \exp (-j/K_w)]^2\}$$

To provide a comparison, both the Oida equation, Eq. [25], and the Wong equation, Eq. [26], were used to process all the shear curves obtained at the two test sites. A summary of the shear strength parameters of the terrain at the two test sites is given in Tables 3 and 4. The first column in the tables identifies the date and the test area. The shear strength parameters c and ϕ in the Mohr-Coulomb equation were determined from the experimentally determined maximum shear stress and the corresponding normal pressure. The value of K_w, which is the shear displacement where the maximum shear stress occurs, is identified from the shear curves experimentally obtained. Both the values of K_r in the Oida and Wong equations are listed. They are obtained from two different optimization procedures. For the Oida equation, a relatively time-consuming iterative procedure was used to obtain the optimum value of K_r that minimizes the error in curve fitting. For the Wong equation, the optimum value of K_r can be directly determined using Eq. [28]. The reference number in the tables refers to the identification number of the data sets of the terrain density and moisture given in Appendix B. Since the shear tests were carried out on the terrain surface, the wet density, dry density and moisture content shown in the tables are the mean values obtained from the data sets, identified by the reference number, at a depth of 5 cm. Both the internal shearing characteristics of the terrain and the rubber-terrain shearing characteristics were obtained at the test sites, and the shear strength parameters for these two types of shearing are identified by I and R, respectively, in Tables 3 and 4.

Table 3. Summary of shear strength parameters - Prescott Site #1

Date (Area)	c (kN/m^2)	ϕ (deg.)	K_w (cm)	K_r (Oida)	K_r (Wong)	Type	Ref. no.	Wet density (kg/m^3)	Dry density (kg/m^3)	Moisture content (%)
Apr. 16 (1-A)	2.2	39.4	6.1	0.655	0.659	I	16-8 16-9	1468	984	49.4
Apr. 19 (1-B)	3.3	33.7	9.3	0.832	0.835	I	19-1 19-2	1549	1028	50.1
	2.8	33.4	7.1	0.673	0.724	I	19-3 19-4	1497	923	62.2
	1.1	33.5	3.6	0.435	0.497	I	19-5	1479	961	53.9
Apr. 22 (1-C)	3.4	24.1	4.9	0.457	0.557	I	22-5 22-6	1646	1069	54.2
	2.6	29.1	4.8	0.366	0.481	I	22-6 22-7	1641	1041	58.1
Apr. 23 (1-D)	5.1	25.6	3.6	0.392	0.448	I	23-1 23-2	1445	1080	34.0
	4.3	22.7	3.5	0.420	0.462	I	23-2 23-3	1459	1048	39.3
	2.7	26.1	4.2	0.411	0.456	I	23-3 23-4	1441	1020	41.3
Apr. 26 (1-E)	2.5	28.2	4.1	0.323	0.379	I	26-6	1384	1064	30.0
	3.1	22.4	3.6	0.779	0.787	R	26-7	1471	1120	31.3
	0.6	31.4	4.5	0.784	0.787	R	26-7	1471	1120	31.3
	0.3	33.1	1.9	0.710	0.714	R	26-8	1623	1118	45.1
	3.0	28.5	2.7	0.637	0.645	R	26-9	1612	1089	47.9

Density and moisture data for depth of 5 cm.

Type: I - Internal shearing; R - Rubber shearing.

Table 4. Summary of shear strength parameters - Prescott Site #2

Date (Area)	c (kN/m^2)	ϕ (deg.)	K_w (cm)	K_r (Oida)	K_r (Wong)	Type	Ref. no.	Wet density (kg/m^3)	Dry density (kg/m^3)	Moisture content (%)
Apr. 27	1.3	25.8	3.1	0.734	0.742	R	27-1	1536	1115	37.8
(2-A)	0.4	33.6	2.4	0.704	0.707	R	27-2	1552	1057	46.9
	3.7	29.8	4.1	0.300	0.382	I	27-3	1551	1053	48.5
	3.2	30.5	4.2	0.359	0.413	I	27-3	1551	1032	48.5
Apr. 29	6.1	26.6	4.5	0.325	0.398	I	29-1	1664	1125	47.9
(2-C)	6.2	30.3	4.7	0.349	0.419	I	29-2	1653	1226	34.8
	1.8	32.2	2.7	0.716	0.721	R	29-3	1383	846	63.4
	1.7	32.0	3.2	0.666	0.678	R	29-4	1596	1019	56.6
Apr. 30	0.0	36.7	4.6	0.683	0.689	R	30-3	1272	1061	20.1
(2-D)	0.3	36.6	6.1	0.806	0.767	R	30-4	1218	987	23.4
	3.1	29.8	3.8	0.396	0.439	I	30-2	1190	876	30.5

Density and moisture data for depth of 5 cm.
Type: I - Internal shearing; R - Rubber shearing.

6. REPETITIVE LOADING TESTS

When a vehicle is in motion, an element of the terrain is subject to the repetitive loading of the consecutive wheels. The response of the terrain to repetitive loading should, therefore, be taken into account in predicting the overall performance of the vehicle.

The response to repetitive loading of the terrain at the two test sites was measured using a bevameter together with the portable automatic data processing system. Figure 17 shows the general features of the response of the terrain to repetitive loading. It can be seen that when the load applied to the terrain is reduced at A, the load-sinkage relationship follows a very steep inclined line AB. This indicates that, during unloading, there is very little elastic rebound. In other words, the terrain exhibits essentially plastic behaviour. When the load is reapplied at B, the pressure-sinkage relationship follows more or less the same path as that during unloading. When the reapplied load exceeds that at which the preceding unloading cycle begins (point A in Fig. 17), additional sinkage results. With the further increase of load, the load sinkage relation appears to follow that under continuous loading as AC shown in Fig. 17. The characteristics of the second unloading-reloading cycle which begins at C are quite similar to those of the first one.

Based on experimental observations described above, the response of the terrain to repetitive loading may be idealized as follows. When the terrain is subject to uninterrupted loading such as OA and AC shown in Fig. 17, the pressure sinkage relationship may be described by the Bekker, the Reece or other similar equations. The pressure-sinkage relation during the reloading cycle (such as BAC shown in Fig. 17), which would provide a basis for the prediction of the sinkage of consecutive wheels, could also be described by the Bekker or Reece equation. Consequently, the pressure-sinkage constants for the reloading cycle could, in principle, be derived using procedures similar to those described in Section 4. However, the values of the pressure-sinkage constants for the reloading cycle will be quite different from those for the virgin terrain, since the shape of the curve BAC is quite different from that of the curve OAC shown in Fig. 17.

The application of the results of repetitive loading tests to the prediction of multi-pass performance of vehicle running gear has been verified to a certain extent (9). It should be mentioned, however, the results described above can only be applied to the evaluation of multi-pass performance of vehicle running gear without aggressive lugs (or grousers) and at low slips. For a running gear with aggressive lugs and operating at high slips, the top layer of the terrain in the rut may be loosened considerably by the running gear. These factors should be taken into account when predicting the multi-pass performance of a vehicle running gear with aggresive lugs and at high slips.

TTRL DATE: 16/04/82

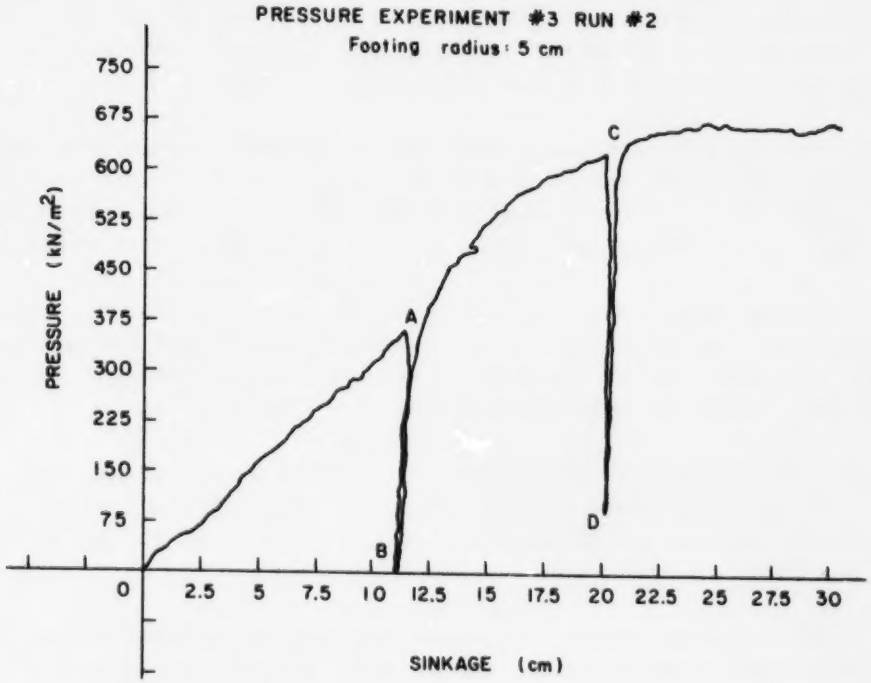

Figure 17. Response to repetitive loading of the terrain at Site 1

7. REMARKS

(a) The pressure-sinkage relationships, the shearing characteristics and the behaviour under repetitive loading of the terrain at two sites for a poplar plantation in Grenville County, near Prescott, Ontario, have been measured, and representative data have been obtained.

(b) The pressure-sinkage relationships of the terrain have been characterized using the Bekker and Reece equations. From the test data, the values of the pressure-sinkage constants for each test area have been derived using a weighted, least-squares method, developed at Carleton.

(c) The shearing characteristics of the terrain have been modelled using a new exponential equation. It has been shown that the new model works well for the type of terrain tested. The shear strength parameters for each test area have been derived from shear test data.

(d) From the results of repetitive loading tests, it has been found that little elastic rebound occurs during unloading for the terrain tested. It appears the pressure-sinkage relationship during the reloading cycle may also be described by the Bekker or Reece equation.

(e) Some preliminary correlations between the mechanical and physical properties of the terrain tested can be made from the field data collected. However, owing to the limited scope of the present study, the quantity of test data obtained is small. Consequently, a comprehensive statistical analysis of the data is not possible.

REFERENCES

1. J.Y. Wong, M. Garber, J.R. Radforth, and J.T. Dowell. Characterization of the mechanical properties of muskeg with special reference to vehicle mobility. J. Terramech. 16(4): 163-180; 1979.

2. J.Y. Wong. Data processing methodology in the characterization of the mechanical properties of terrain. J. Terramech. 17(1): 13-41; 1980.

3. J.Y. Wong, P.S. Harris, and J. Preston-Thomas. Development of a portable automatic data processing system for terrain evaluation. Proceedings of the 7th International Conference of the International Society for Terrain-Vehicle Systems, Calgary, Alberta, Canada, 1981. Vol. III, pp. 1067-1092.

4. J.Y. Wong, J.R. Radforth, and J. Preston-Thomas. Some further studies on the mechanical properties of muskeg in relation to vehicle mobility. J. Terramech. 19(2): 1982.

5. M.G. Bekker. Theory of Land Locomotion. The University of Michigan Press, 1956.

6. M.G. Bekker. Introduction to Terrain-Vehicle Systems. The University of Michigan Press, 1969.

7. V.V. Kacigin and V.V. Guskov. The basis of tractor performance theory. J. Terramech. 5(3): 43-66; 1968.

8. A. Oida. Study on equation of shear stress-displacement curves. Technical Report No. 5, Farm Power and Machinery Laboratory, Kyoto University, Japan, 1979.

9. J.Y. Wong. Prediction of multiple-pass performance of tires - A review. Proceedings of the 6th International Conference of the International Society for Terrain-Vehicle Systems, Vienna, Austria, 1978. Vol. II, pp. 541-553.

APPENDIX A. KEY TO SOIL CLASSIFICATIONS

Table A1. Key to soil classification

	Medium textured till	Fine textured lacustrine	Well sorted outwash	
Natural drainage	Good	Poor	Good	Imperfect
Series, acreage type and symbol	Grenville (50,500) loam	North Gower (6,400) clay loam	Uplands (18,000) sandy loam	Rubicon (35,000) sandy loam
Topography	Undulating to rolling	Level to slightly undulating	Strongly undulating to rolling	Undulating to level
Surface stoniness	Moderately stony to bouldery	Stonefree	Stonefree	Stonefree
Surface reaction	About neutral	About neutral	Moderately to slightly acid	Moderately to slightly acid
Great soil group	Brown Forest	Dark grey Gleisolic	Podsol	Ground Water Podsol
Profile description of cultivated soil	6 inches dark brown loam underlain by reddish brown loam underlain by dark brown loam and clay loam over greyish brown calcareous till	5-6 inches very dark grey clay loam underlain by grey mottled clay loam over grey and yellow mottled clay and grading into grey plastic clay	3-4 inches light brown sand and sandy loam underlain by yellowish brown sand over coarse grey sand with some carbonates	4-6 inches dark grey sand and sandy loam underlain by reddish brown sandy loam over grey sand. Occasionally the grey podsol layer shows in freshly plowed fields but usually becomes incorporated with the other horizons when cultivated

Source: Soil Survey by the Department of Soils, Ontario Agricultural College, Guelph, and the Experimental Farms Service, Dominion Department of Agriculture, Ottawa.

APPENDIX B. WET DENSITY, DRY DENSITY, AND MOISTURE CONTENT OF TEST AREAS

Table B1. Summary of density and moisture measurements

Date	Area	Ref. no.	Depth (cm)	Wet density (kg/m^3)	Dry density (kg/m^3)	Moisture content (%)
Apr. 16	1-A	16-1	5	1535	988	55.3
			10	1546	1004	53.7
			15	1543	1008	53.0
			20	1544	1008	53.3
			25	1552	1020	52.2
			30	1578	1033	52.7
		16-2	5	1586	1075	47.6
			10	1604	1097	46.2
			15	1626	1125	44.5
			20	1607	1101	46.1
			25	1608	1102	46.0
			30	1626	1118	45.3
		16-3	5	1554	998	55.7
			10	1548	998	55.0
			15	1538	995	54.6
			20	1519	977	55.4
			25	1514	955	58.4
			30	1517	971	56.2
		16-4	5	1493	993	50.4
			10	1490	993	49.9
			15	1517	1019	48.8
			20	1503	1000	50.4
			25	1509	1000	51.0
			30	1527	1027	48.7
		16-5	5	1514	1014	49.4
			10	1532	1038	47.6
			15	1560	1070	45.8
			20	1581	1067	48.0
			25	1597	1107	44.2
			30	1621	1115	45.4

Table B1 (Continued)

Date	Area	Ref. no.	Depth (cm)	Wet density (kg/m^3)	Dry density (kg/m^3)	Moisture content (%)
Apr. 16	1-A	16-6	5	1458	942	54.7
			10	1483	982	51.1
			15	1491	974	53.1
			20	1559	1038	50.1
			25	1589	1089	45.9
			30	1624	1112	46.1
		16-7	5	1464	969	51.2
			10	1485	984	51.1
			15	1565	1077	45.4
			20	1576	1077	46.5
			25	1573	1094	43.8
			30	1567	1061	47.6
		16-8	5	1456	961	51.6
			10	1459	969	50.6
			15	1512	1030	46.8
			20	1557	1069	45.7
			25	1567	1078	45.3
			30	1573	1075	46.4
		16-9	5	1480	1006	47.2
			10	1532	1062	44.3
			15	1559	1072	45.4
			20	1570	1094	43.5
			25	1567	1077	45.5
			30	1599	1123	42.5
Apr. 19	1-B	19-1	5	1467	968	51.6
			10	1490	988	50.7
			15	1504	996	50.9
			20	1520	1011	50.5
			25	1533	1033	48.3
			30	1557	1062	46.6
		19-2	5	1631	1088	49.9
			10	1642	1115	47.3
			15	1645	1112	48.0
			20	1618	1085	49.2
			25	1596	1069	49.2
			30	1621	1089	48.9

Table B1 (Continued)

Date	Area	Ref. no.	Depth (cm)	Wet density (kg/m^3)	Dry density (kg/m^3)	Moisture content (%)
Apr. 19	1-B	19-3	5	1479	932	58.5
			10	1469	923	59.1
			15	1482	940	57.5
			20	1474	924	59.4
			25	1488	961	54.9
			30	1554	1024	51.6
		19-4	5	1515	913	65.8
			10	1507	915	64.9
			15	1527	924	65.2
			20	1538	952	61.5
			25	1560	966	61.4
			30	1580	995	58.7
		19-5	5	1479	961	53.9
			10	1533	1024	49.9
			15	1576	1067	47.7
			20	1512	996	51.8
			25	1548	1043	48.3
			30	1594	1091	46.0
		19-6	5	1458	1012	44.0
			10	1456	1008	44.6
			15	1447	998	44.8
			20	1466	1003	46.2
			25	1479	1033	43.0
			30	1543	1094	41.0
		19-7	5	1461	1011	44.4
			10	1445	982	47.1
			15	1461	1009	44.6
			20	1506	1056	42.7
			25	1538	1099	40.7
			30	1591	1134	40.3
		19-8	5	1530	1045	46.5
			10	1551	1054	47.1
			15	1543	1057	46.0
			20	1532	1051	45.8
			25	1544	1035	49.1
			30	1604	1115	43.7

Table B1 (Continued)

Date	Area	Ref. no.	Depth (cm)	Wet density (kg/m^3)	Dry density (kg/m^3)	Moisture content (%)
Apr. 22	1-C	22-1	5	1602	1036	54.5
			10	1626	1053	54.6
			15	1647	1089	51.2
			20	1660	1093	51.9
			25	1684	1109	51.8
			30	1717	1153	48.9
		22-2	5	1594	1004	58.5
			10	1660	1075	54.3
			15	1692	1112	52.2
			20	1700	1102	54.2
			25	1721	1131	52.0
			30	1753	1155	51.7
		22-3	5	1666	1129	47.6
			10	1672	1149	45.6
			15	1706	1161	47.0
			20	1729	1200	44.0
			25	1757	1229	43.0
			30	1794	1250	43.5
		22-4	5	1642	1073	52.9
			10	1668	1096	52.2
			15	1682	1112	51.4
			20	1656	1088	52.3
			25	1682	1107	51.9
			30	1689	1117	51.2
		22-5	5	1629	1032	57.9
			10	1676	1059	58.3
			15	1689	1073	57.4
			20	1701	1089	56.1
			25	1719	1107	55.2
			30	1743	1137	53.2
		22-6	5	1663	1105	50.4
			10	1703	1136	49.9
			15	1708	1120	52.4
			20	1719	1149	49.6
			25	1719	1147	49.8
			30	1756	1187	47.9

Table B1 (Continued)

Date	Area	Ref. no.	Depth (cm)	Wet density (kg/m^3)	Dry density (kg/m^3)	Moisture content (%)
Apr. 22	1-C	22-7	5	1621	977	65.7
			10	1679	1028	63.2
			15	1732	1101	57.4
			20	1757	1120	57.0
			25	1757	1099	60.0
			30	1801	1158	55.5
Apr. 23	1-D	23-1	5	1400	1097	27.7
			10	1408	1102	27.7
			15	1426	1115	27.9
			20	1471	1144	28.6
			25	1543	1242	24.3
			30	1594	1283	24.1
		23-2	5	1490	1062	40.3
			10	1524	1104	38.1
			15	1572	1157	36.0
			20	1592	1185	34.3
			25	1612	1202	34.1
			30	1634	1210	35.2
		23-3	5	1427	1033	38.2
			10	1485	1093	35.8
			15	1485	1096	36.4
			20	1559	1153	35.1
			25	1658	1246	33.0
			30	1689	1288	31.0
		23-4	5	1455	1008	44.3
			10	1477	1033	42.9
			15	1509	1070	41.0
			20	1543	1110	39.0
			25	1564	1123	39.2
			30	1608	1169	37.5
		23-5	5	1650	1248	32.1
			10	1650	1250	31.9
			15	1668	1272	31.9
			20	1716	1307	31.2
			25	1730	1318	31.2
			30	1764	1349	30.7

Table B1 (Continued)

Date	Area	Ref. no.	Depth (cm)	Wet density (kg/m^3)	Dry density (kg/m^3)	Moisture content (%)
Apr. 26	1-E	26-1	5	1467	1035	31.7
			10	1491	1153	29.3
			15	1512	1160	30.3
			20	1507	1152	30.8
			25	1501	1152	30.3
			30	1544	1184	30.5
		26-2	5	1394	1097	26.9
			10	1418	1118	26.8
			15	1455	1158	25.6
			20	1488	1190	25.1
			25	1517	1211	25.2
			30	1540	1237	24.5
		26-3	5	1392	1105	26.0
			10	1402	1109	26.4
			15	1391	1097	26.6
			20	1413	1121	26.1
			25	1459	1169	24.9
			30	1504	1221	23.3
		26-4	5	1472	1128	30.5
			10	1479	1123	31.6
			15	1528	1181	29.5
			20	1592	1251	27.3
			25	1594	1242	28.5
			30	1602	1243	28.8
		26-5	5	1480	1096	35.0
			10	1466	1067	37.4
			15	1453	1051	38.3
			20	1459	1059	37.9
			25	1488	1096	35.7
			30	1512	1123	34.8
		26-6	5	1384	1064	30.0
			10	1394	1086	28.3
			15	1392	1080	28.9
			20	1408	1096	28.5
			25	1463	1153	26.8
			30	1514	1193	26.9

Table B1 (Continued)

Date	Area	Ref. no.	Depth (cm)	Wet density (kg/m^3)	Dry density (kg/m^3)	Moisture content (%)
Apr. 26	1-E	26-7	5	1471	1120	31.3
			10	1493	1149	30.0
			15	1543	1205	28.1
			20	1591	1245	27.8
			25	1632	1285	27.0
			30	1663	1317	26.4
		26-8	5	1623	1118	45.1
			10	1608	1107	45.1
			15	1604	1105	44.9
			20	1620	1121	44.5
			25	1661	1163	42.7
			30	1689	1184	42.6
		26-9	5	1612	1089	47.9
			10	1623	1107	46.5
			15	1637	1109	47.6
			20	1655	1105	49.7
			25	1652	1128	46.4
			30	1700	1176	44.6
Apr. 27	2-A	27-1	5	1536	1115	37.8
			10	1604	1166	37.4
			15	1610	1174	37.0
			20	1573	1133	38.9
			25	1605	1176	36.5
			30	1632	1198	36.3
		27-2	5	1552	1057	46.9
			10	1568	1062	46.9
			15	1584	1077	47.2
			20	1549	1049	47.7
			25	1556	1045	48.9
			30	1596	1105	44.4
		27-3	5	1551	1045	48.5
			10	1578	1057	49.3
			15	1592	1061	50.1
			20	1608	1080	48.9
			25	1605	1091	47.0
			30	1669	1152	44.9

Table B1 (Continued)

Date	Area	Ref. no.	Depth (cm)	Wet density (kg/m^3)	Dry density (kg/m^3)	Moisture content (%)
Apr. 27	27-4	2-A	5	1533	1091	40.5
			10	1541	1083	42.2
			15	1557	1105	40.9
			20	1567	1120	39.9
			25	1596	1155	38.2
			30	1684	1229	37.0
Apr. 28	2-B	28-1	5	1604	1102	45.5
			10	1644	1129	45.5
			15	1676	1165	44.0
			20	1685	1176	43.3
			25	1690	1185	42.6
			30	1705	1197	42.6
		28-2	5	1637	1094	49.5
			10	1685	1147	46.8
			15	1714	1179	45.3
			20	1677	1133	48.2
			25	1689	1139	48.3
			30	1705	1149	48.3
		28-3	5	1709	1173	45.7
			10	1709	1179	44.9
			15	1737	1208	43.9
			20	1767	1245	41.9
			25	1749	1222	43.1
			30	1772	1253	41.4
Apr. 29	2-C	29-1	5	1664	1125	47.9
			10	1711	1165	46.8
			15	1735	1187	46.1
			20	1751	1219	43.7
			25	1765	1222	44.4
			30	1772	1218	45.6
		29-2	5	1653	1226	34.8
			10	1693	1280	32.2
			15	1640	1227	33.6
			20	1576	1157	36.3
			25	1652	1229	34.5
			30	1706	1283	33.0

Table B1 (Continued)

Date	Area	Ref. no.	Depth (cm)	Wet density (kg/m^3)	Dry density (kg/m^3)	Moisture content (%)
Apr. 29	2-C	29-3	5	1383	846	63.4
			10	1511	961	57.2
			15	1580	1030	53.3
			20	1586	1046	51.5
			25	1572	1024	53.6
			30	1615	1073	50.4
		29-4	5	1596	1019	56.6
			10	1605	1035	55.2
			15	1589	1008	57.7
			20	1615	1041	55.1
			25	1636	1065	53.6
			30	1666	1089	53.0
		29-5	5	1552	1045	48.6
			10	1612	1094	47.3
			15	1599	1093	46.4
			20	1580	1064	48.9
			25	1645	1139	44.5
			30	1680	1161	44.7
Apr. 30	2-D	30-1	5	1224	988	23.7
			10	1291	1065	21.3
			15	1336	1110	20.4
			20	1360	1126	20.7
			25	1448	1218	19.0
			30	1515	1280	18.5
		30-2	5	1190	876	30.5
			10	1173	902	30.2
			15	1234	961	28.3
			20	1291	1012	27.5
			25	1399	1125	24.3
			30	1471	1203	22.3
		30-3	5	1272	1061	20.1
			10	1326	1121	18.4
			15	1224	1014	20.6
			20	1339	1133	18.2
			25	1456	1240	17.4
			30	1495	1288	16.1

Table B1 (Concluded)

Date	Area	Ref. no.	Depth (cm)	Wet density (kg/m^3)	Dry density (kg/m^3)	Moisture content (%)
Apr. 30	2-D	30-4	5	1218	987	23.4
			10	1309	988	21.5
			15	1358	1139	19.3
			20	1174	955	23.0
			25	1474	1251	17.8
			30	1556	1330	16.9